Available online at www.sciencedirect.com
ScienceDirect
Ceramics International 37 (2011) 2711–2717
CERAMICS INTERNATIONAL
www.elsevier.com/locate/ceramint

Microstructure, mechanical properties and thermal shock resistance of plasma sprayed nanostructured zirconia coatings

G. Di Girolamo [a,*], F. Marra [b], C. Blasi [a], E. Serra [c], T. Valente [b]

[a] ENEA, UTTMATB, Brindisi Research Centre, 72100 Brindisi, Italy
[b] Department of Chemical and Materials Engineering, University of Rome "La Sapienza" – UdR INSTM Roma "La Sapienza", 00184 Rome, Italy
[c] ENEA, UTTMAT, Casaccia Research Centre, 00123 Rome, Italy

Received 28 February 2011; received in revised form 11 April 2011; accepted 12 April 2011
Available online 16 April 2011

Abstract

Nanostructured yttria stabilized zirconia (YSZ) coatings were deposited by Atmospheric Plasma Spraying (APS). X-ray diffraction (XRD) was used to investigate their phase composition, while scanning electron microscopy (SEM) was employed to examine their microstructure. The coatings showed a unique and complex microstructure composed of well-melted splats with columnar crystal structure, partially melted areas, which resembled the morphology of the powder feedstock, and equiaxed grains. Vickers microhardness of nanostructured zirconia coatings was similar to that of the conventional ones and strongly depended on the indentation load. Otherwise, a higher thermal shock resistance was found. This effect was addressed to the retention of nanostructured areas in coating microstructure and to the corresponding high porosity.

Keywords: C. Hardness; C. Thermal shock resistance; D. ZrO_2; E. Thermal applications; Plasma spraying

1. Introduction

Thermal barrier coatings (TBCs) are commonly used to thermally insulate metallic hot-section components of aircraft and land-based turbine engines, in order to increase their durability as well as to improve the efficiency [1,2]. TBCs materials have to satisfy some basic requirements, such as low thermal conductivity, high-temperature phase stability, high thermal expansion coefficient (CTE) and low Young's modulus [3]. Actually, yttria partially stabilized zirconia is well-recognized as the best candidate for TBCs, because it provides a good compromise between the main requirements demanded to TBC materials and generally offers a satisfactory performance [4–8].

However, new concepts suggest the study of new architectures and new materials. Nanostructured materials seem to be particularly promising due to their enhanced hardness, strength and toughness [9]. It has been reported that nanostructured zirconia coatings show lower thermal conductivity, lower Young's modulus, higher CTE and higher toughness with respect to the microstructured conventional ones [10–12].

In the present work nanostructured zirconia coatings were fabricated by APS. The starting powder particles were partially melted in order to restrict the effects of nucleation and grain growth, so that their original nanostructure was preserved [13–15]. Indeed, when these particles are fully melted the original nanostructure is destroyed and the coating tends to behave as a conventional one.

XRD and SEM were employed for phase analysis and microstructural characterisation of as-sprayed nanostructured YSZ coatings, respectively. Microhardness measurements were performed on the polished cross section of the deposits. Thermal shock resistance of nanostructured zirconia coatings was also investigated.

2. Materials and methods

Plasma spraying was carried out using an APS system equipped with a F4-MB plasma torch with 6 mm internal diameter nozzle (Sulzer Metco, Wolhen, Switzerland). Stainless steel plates ($150 \times 25 \times 3$ mm^3) were used as substrates.

* Corresponding author.
E-mail address: giovanni.digirolamo@enea.it (G. Di Girolamo).

0272-8842/$36.00
doi:10.1016/j.ceramint.2011.04.024

Before spraying, they were grit-blasted with alumina abrasive powder (Metcolite F, Sulzer Metco, Westbury, NY) to increase the surface roughness and to achieve proper mechanical interlocking between the coatings and the same substrates. Then they were ultrasonically cleaned in ethanol, placed on a rotating sample holder and coated with 250 μm thick coatings. The nanostructured ZrO_2–7 wt.% Y_2O_3 powder feedstock (Nanox S4007, Inframat Corporation, North Haven, CT) was deposited using the spraying parameters listed in Table 1. In order to reduce the thermal expansion mismatch between the substrate and the TBC, a bond coat was deposited using a commercial CoNiCrAlY powder (Amdry 995C, Sulzer Metco, Westbury, NY). The bond coat was 100 μm thick.

The deposition efficiency was calculated from the ratio between the coating mass and the feedstock mass delivered to the plasma torch. This last was determined from the powder feed rate and the spraying time on the substrate. Therefore, the deposition rate was 9.6 ± 0.2 μm per torch pass, while the deposition efficiency was $47.2 \pm 1.0\%$.

The phase composition of both nanostructured zirconia feedstock and as-sprayed coatings was investigated using an X-ray powder diffractometer (PW 1880, Philips, Almelo, Netherlands) operating with CuKα radiation ($\lambda = 0.154186$ nm) produced at 40 kV and 40 mA. The analyzed range of the diffraction angle 2θ was between 20 and 80°, by a step width of 0.01° and a time per step equal to 5 s.

The morphology and the microstructure of both the nanostructured feedstock and coatings were analyzed by SEM-FEG (Field Emission Gun, Leo Gemini mod. 1530, Carl Zeiss, Oberkochen, Germany) equipped with high-resolution secondary electron detector (in-lens detector). Both fractured surface and cross section of YSZ coatings were observed in as-deposited state, whereas the polished cross section was prepared using proper metallographic procedure. Each coating was cut using a low-speed diamond saw, cold mounted in vacuum in two-part epoxy resin and polished up to 0.5 μm. SEM pictures at magnifications between 200× and 1000× were processed by an image analysis software (Image J, U.S. National Institutes of Health, Bethesda, MD), in order to measure the percentage of unmelted areas and the total porosity of nanostructured YSZ coatings.

Microhardness measurements were carried out on their polished cross section, using a Vickers microindenter (VMHT MOT, Leica Microsystems, Weztlar, Germany). The indentations were performed at 50 and 100 gf loads for a dwell time of 15 s. The spacing between the indentations was kept at least three times the diagonal to avoid further stresses produced by the interaction between consecutive indentations. The microhardness data were analyzed by Weibull statistics.

Thermal shock tests were performed on 12 coated specimens ($55 \times 7.5 \times 3.5$ mm^3). The samples were heated at 1020 °C in an air tubular oven (Lenton Thermal Design Limited), hold at this temperature for 5 min and then rapidly quenched in ambient temperature water. During the tests the coating surface was analyzed step by step, in order to evaluate the gradual damaging promoted by cracking and delamination. The images were acquired using a stereomicroscope (Leica MS 5) and the image analysis software mentioned above. The thermal shock resistance was quantified by recording the number of thermal shock cycles up to failure.

Table 1
Plasma spraying parameters used in this work.

Process parameters	Amdry 995C	Nanox S4007
Arc current (A)	600	600
Voltage (V)	71.4	68.8
Turntable speed (rpm)	50	150
Substrate tangential speed (mm s^{-1})	1041	3124
Gun speed (mm s^{-1})	4	4
Primary gas Ar flow rate (slpm)	55	40
Secondary gas H_2 flow rate (slpm)	11	12
Spray distance (mm)	120	100
Carrier gas flow rate (slpm)	3	2.8
Powder feed rate (g min^{-1})	49.7	28.5
Injector diameter (mm)	1.8	1.8
Injector angle (°)	90	90
Distance torch-injector (mm)	6	5

slpm, standard litres per minute.

3. Results and discussion

3.1. Phase composition

X-ray diffraction patterns of YSZ powder and as-sprayed coating are shown in Fig. 1a. The feedstock is mainly composed of tetragonal t zirconia with smaller amounts of cubic c and monoclinic m zirconia phases, according to Joint Committee on Powder Diffraction Standards (JCPDS) available at International Centre for Diffraction Data (no. 81-1544 for tetragonal zirconia, no. 49-1642 for cubic zirconia and no. 371484 for monoclinic zirconia). The coating is composed of a mixture of non-trasformable tetragonal t′ and tetragonal t zirconia phases, as illustrated in high-angle region (72–75°) of the diffraction pattern, where an example for the profile fit of (4 0 0) zirconia reflections is shown (see Fig. 1b). The formation of the metastable tetragonal t′ phase is promoted by the high quenching rate (10^6–10^7 K s^{-1}) of the molten droplets, while the tetragonal t phase is associated to the retained unmelted particles embedded in coating microstructure, as discussed in the next section. The amount of tetragonal t zirconia is 22.5% (t′ phase = 77.5%). No monoclinic phase is noticed in as-sprayed coating, because it was transformed to t′ phase upon melting.

3.2. Microstructure

Fig. 2 shows the morphology of spray-dried agglomerated particles. Their size is between 15 and 150 μm, as reported by the manufacturer. The right inset shows the morphology of single YSZ nanoclusters. Five feedstock samples were considered for grain size measurements. The grain size is in the range between 30 and 200 nm, as illustrated in detail of Fig. 2. Single nanoparticles have to be agglomerated because they are unable to be carried in the plasma plume, due to their low mass, and thus deposited on a substrate [13]. The intrinsic

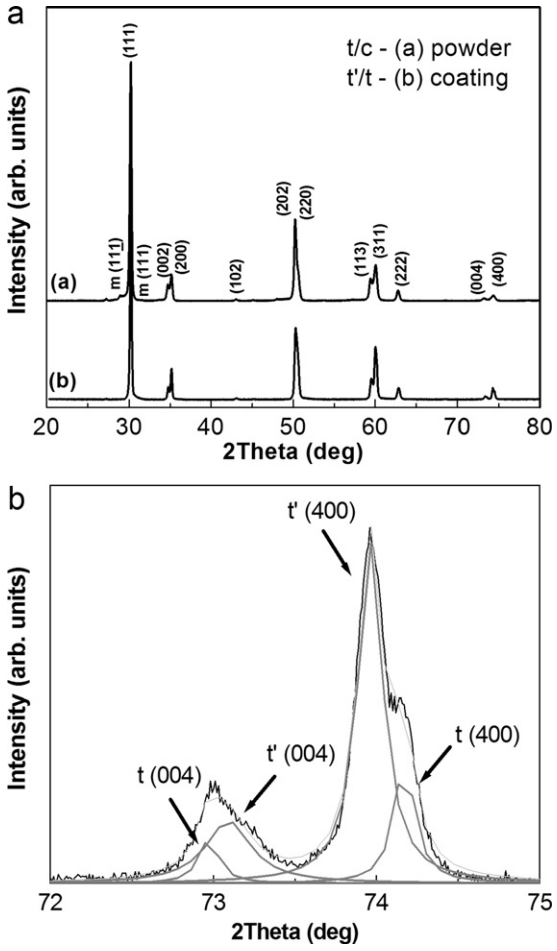

Fig. 1. (a) Shows the XRD patterns of (a) nanostructured YSZ powder and (b) as-sprayed coating. (b) Shows the high-angle region of the diffraction pattern of as-sprayed coating.

porosity produced during the agglomeration process affects the coating microstructure. Indeed, during plasma spray deposition, hot gas mixture penetrates inside agglomerated particles and melts their surface. Due to the heating of the gas herein entrapped, the agglomerated particles are pressurized and

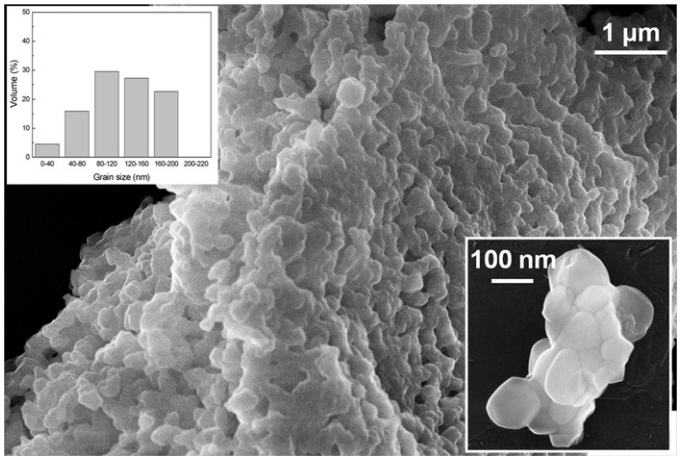

Fig. 2. Morphology of nanostructured zirconia feedstock. The insets show the morphology of YSZ nanoclusters and their size distribution, respectively.

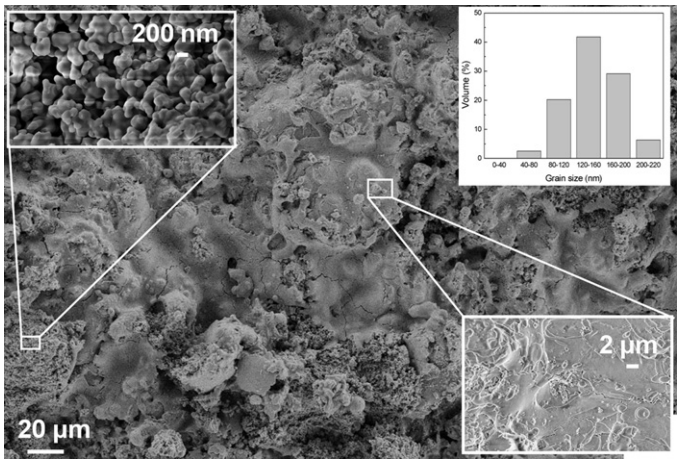

Fig. 3. Surface morphology of nanostructured zirconia coating, containing loose particles and well-melted splats. The graph of grain size distribution is also shown.

eventually destroyed, blowing up into several smaller ones, prior to their impact on the substrate [16]. Their core remains unmelted, so that the grain growth is partially prevented and the starting nanostructure can be retained at room temperature. The short residence time of the sprayed particles in the plasma jet, the low heat transfer associated to their intrinsic porosity and the high cooling rate assist this mechanism [17].

As clearly displayed in Fig. 3, the coating shows two different kinds of microstructures. The details inserted at the opposite corners of the picture illustrate a poorly consolidated area and a well-melted splat, respectively. The former is composed of loosely bound particles, which resemble the morphology of the powder feedstock. In these areas the grain growth does not occur and the particle size distribution is similar to that observed in the starting feedstock, *i.e.* approximately in the range from 40 to 220 nm. It should be noted that the sprayed particles are commonly characterised by different thermal history, depending on the temperature distribution in the plasma jet. Indeed, some particles are heated at lower rate and thus the grain growth typically occurs. These well-melted particles impinge on the substrate at high kinetic energy and are well-flattened, thus producing a smooth surface.

Fig. 4 shows the fractured cross section of nanostructured YSZ coating. It exhibits a complex microstructure where large areas, mainly consisting of unmelted or partially melted particles, are cemented by well-melted splats. These last ones are composed of overlapped lamellae whose thickness is in the range between 0.5 and 3 μm. As clearly displayed in Fig. 5, columnar grains are detectable within the lamellae. They are oriented along the direction of the grain growth and their diameter is approximately in the range between 40 and 300 nm. Their morphology is related to their heterogeneous nucleation at splat boundary and their growth into the molten splat, due to the heat flow released by the crystallization of previously deposited material [18,19]. Otherwise, if the heat loss promoted by cooling at substrate interface is higher than the heat released by the crystallization a homogeneous nucleation occurs and

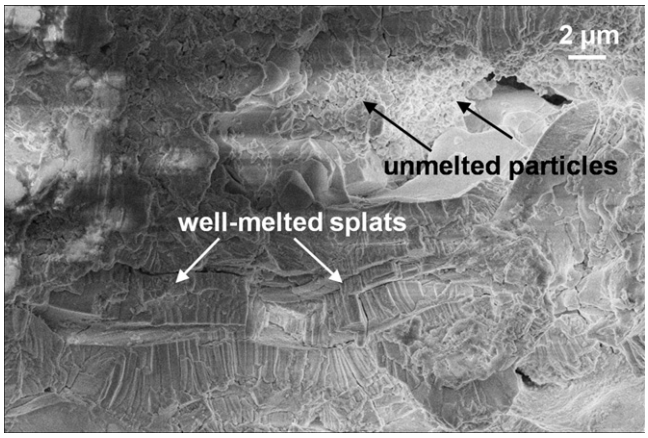

Fig. 4. Microstructure of nanostructured zirconia coating (fractured cross section).

results in the formation of equiaxed grains, as observed in Fig. 5.

Fig. 6a shows the polished cross section of nanostructured YSZ coating. The white arrows denote some retained nanosized areas. Image analysis allows to calculate coating porosity as well as the fractions of well-melted and partially melted nanosized areas. So, the average porosity of nanostructured zirconia coating is equal to 22% (standard deviation = 2.5%), while the amount of retained nanosized areas is equal to 22% (standard deviation = 1.2%). This last value is in perfect agreement with quantitative XRD results. It should be noted that a higher amount of retained nanozones embedded in coating microstructure is generally more suitable for fabrication of abradable coatings [10,20]. The coating shows pores of different size and some microcracks, which result from the release of thermal stresses during cooling. Fine spherical pores smaller than 3 μm derive from gas entrapped in the molten droplets and are homogeneously distributed, while the pores with diameter ranging from 3 to 10 μm are produced by filling structural defects and pull-out effects during grinding and polishing steps. For useful comparison, conventional YSZ coatings have been also produced by using a commercial powder feedstock (Metco 204NS, Sulzer Metco, Westbury, NY) and the spraying parameters reported in a previous work

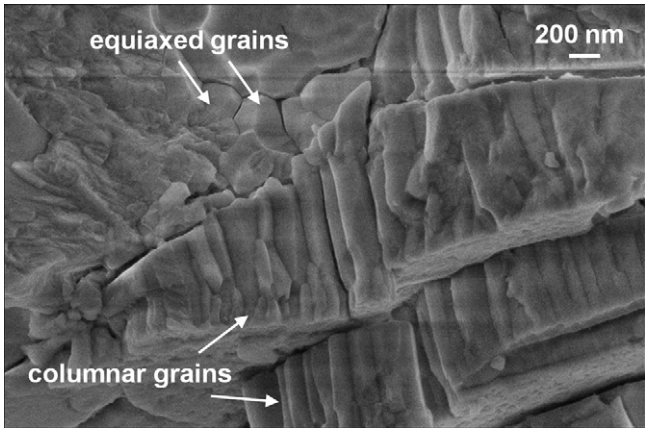

Fig. 5. Coating cross section showing columnar and equiaxed grains.

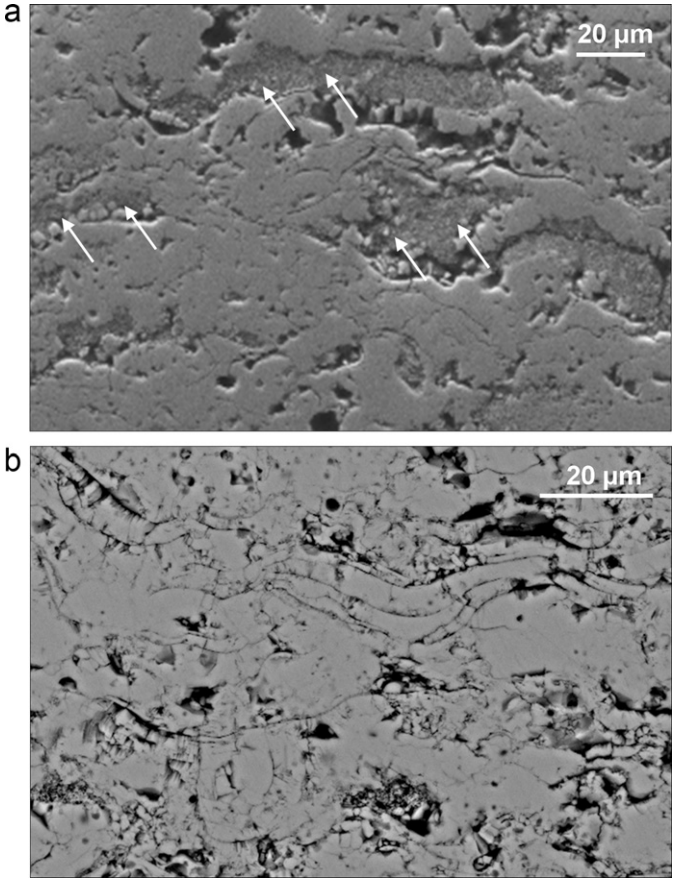

Fig. 6. (a) Shows the polished cross section of nanostructured YSZ coating, while (b) shows the cross sectional microstructure of conventional YSZ coating.

[21]. Fig. 6b shows the cross-sectional lamellar microstructure of plasma sprayed conventional YSZ coating, rich of pores, splat boundaries and microcracks. The presence of more pronounced splat boundaries suggests lower bonding strength with respect to the nanostructured coatings. The total porosity is equal to 12.2 ± 1.5%.

3.3. Microhardness

Vickers indentations were performed on the cross section of nanostructured YSZ coatings. The load of 50 gf has been set in order to avoid cracking in the nanosized areas during indentation. The microhardness average is 939 HV (standard deviation = 188 HV), whereas the extreme values are 434 and 1386 HV, respectively. In Table 2 the microhardness average of nanostructured YSZ coating is compared to those of other nanostructured and conventional coatings [22]. The hardness

Table 2
Microhardness of nanostructured and conventional YSZ coatings.

Coating	Indentation load (gf)	Average hardness (HV)
Nanostructured YSZ	50	939
Conventional YSZ	50	900
Nanostructured YSZ [22]	50	820
Conventional YSZ [22]	50	750

values are higher than those reported in the literature for nanostructured coatings and similar to those found for the conventional coatings tested in this work. In fact, the difference in hardness values is <5%, despite their different microstructures and porosity values.

The microhardness data are broadly distributed due to the presence of microstructural defects such as pores, splat boundaries and microcracks, so that Weibull statistics are employed. The cumulative density function of probability $F(x)$ is represented by Eq. (1):

$$F(x) = 1 - e^{-(x/x_0)^m} \quad (1)$$

where x is the microhardness data, x_0 is the scale parameter giving 63.2% of the cumulative density and m is the Weibull modulus, which reflects the scatter in data distribution. By plotting $\ln(-\ln(1 - F_i))$ versus $\ln(x)$ both m and x_0 parameters can be calculated. Sorting the experimental data in ascending order, the cumulative density of probability F_i assigned to the ith microhardness x_i can be defined as:

$$F_i = \frac{i - 0.5}{n} \quad (2)$$

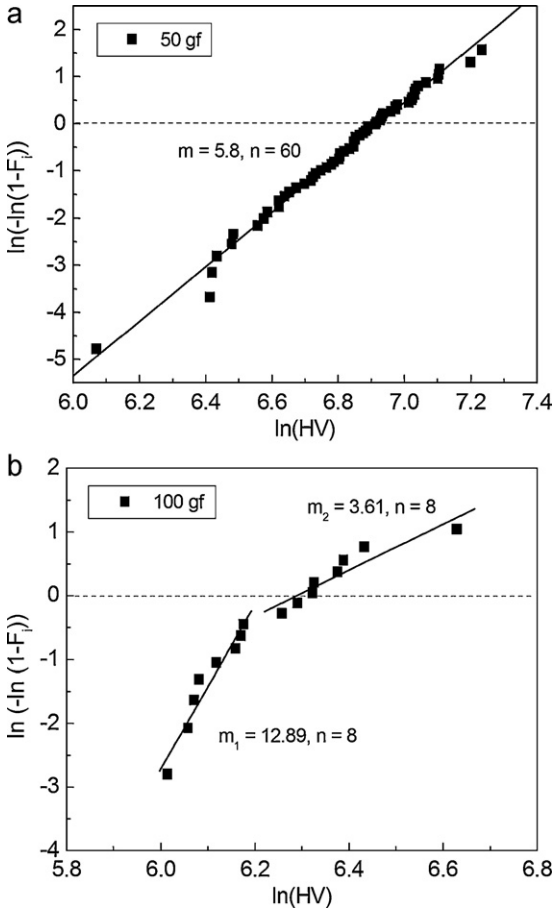

Fig. 7. Weibull plots of microhardness data for nanostructured YSZ coatings tested at (a) 50 and (b) 100 gf, respectively. At the highest load a bimodal distribution is observable.

where n represents the total number of data points [23]. The Weibull plot of the Vickers microhardness data obtained at 50 gf is shown in Fig. 7a.

It is worth noting that, even if nanostructured zirconia coating clearly exhibits a bimodal microstructure, the microhardness data can be directly approximated by single linear fit and the corresponding Weibull modulus is 5.8. Otherwise, a bimodal distribution has been noticed by other investigators at indentations loads ranging from 10 to 50 gf [22,24]. However, by increasing the indentation load up to 100 gf, a sharp decrease in microhardness is found for nanostructured zirconia coating (536 ± 107 HV), while the corresponding hardness average of the conventional coating is 600 HV. As shown in Fig. 7b, a bimodal distribution of microhardness data is noticed, *i.e.* the presence of two different Weibull moduli ($m_1 = 12.9$ and $m_2 = 3.6$). The region of the Weibull plot at higher hardness values reflects the mechanical behaviour of fully melted splats, whereas the region at lower hardness values is representative of zones consisting of unmelted and porous particles embedded in coating microstructure. Therefore, the mechanical behaviour of nanostructured zirconia coatings is strongly related to the melting degree of sprayed particles and to the amount of retained unmelted particles. Moreover, we can deduce that it also depends on their cohesive strength and the effect is emphasized as the indentation load increases, due to the eventual formation of small cracks in the nanosized areas. At higher loads the indentations cover larger areas and thus the extent of the microstructural defects increases.

3.4. Thermal shock resistance

Fig. 8a shows the surface of nanostructured zirconia coating after 40–60 thermal shock cycles, while Fig. 8b shows the same surface after 80–90 cycles. At high temperature the mismatch in thermal expansion coefficients of substrate, bond coat and top coat produces high thermal stresses in the whole TBC system. This effect becomes more significant as the number of cycles increases and gradually promotes the formation and the propagation of significant cracks within the nanostructured YSZ coating. According to the optical examination the appearance of crack networks, which extend to large areas of coating surface, was observable only after 35–40 thermal cycles. These cracks were produced by in-plane tensile stresses, developed in the outer layer of the same coating and promoted by the restriction of the inner layers upon thermal cycling. A partial sintering of the porous microstructure probably assisted this mechanism. Therefore, as observed in Fig. 8a, small isolated areas on the coating surface are delaminated after 40–60 cycles. As shown in Fig. 8b, the delamination of large areas occurs only after 90 cycles. The coating peels off from the inside of the ceramic coating and spalls layer by layer, without any spallation at TBC/bond coat interface. Therefore, this mechanism of damaging is more significant than the formation of a thermally grown oxide (TGO) at TBC/bond coat interface, commonly promoted by high-temperature oxidation of the bond coat surface, *i.e.* the thickness of the TGO is not high enough to promote TBC spallation. After 120 thermal shock

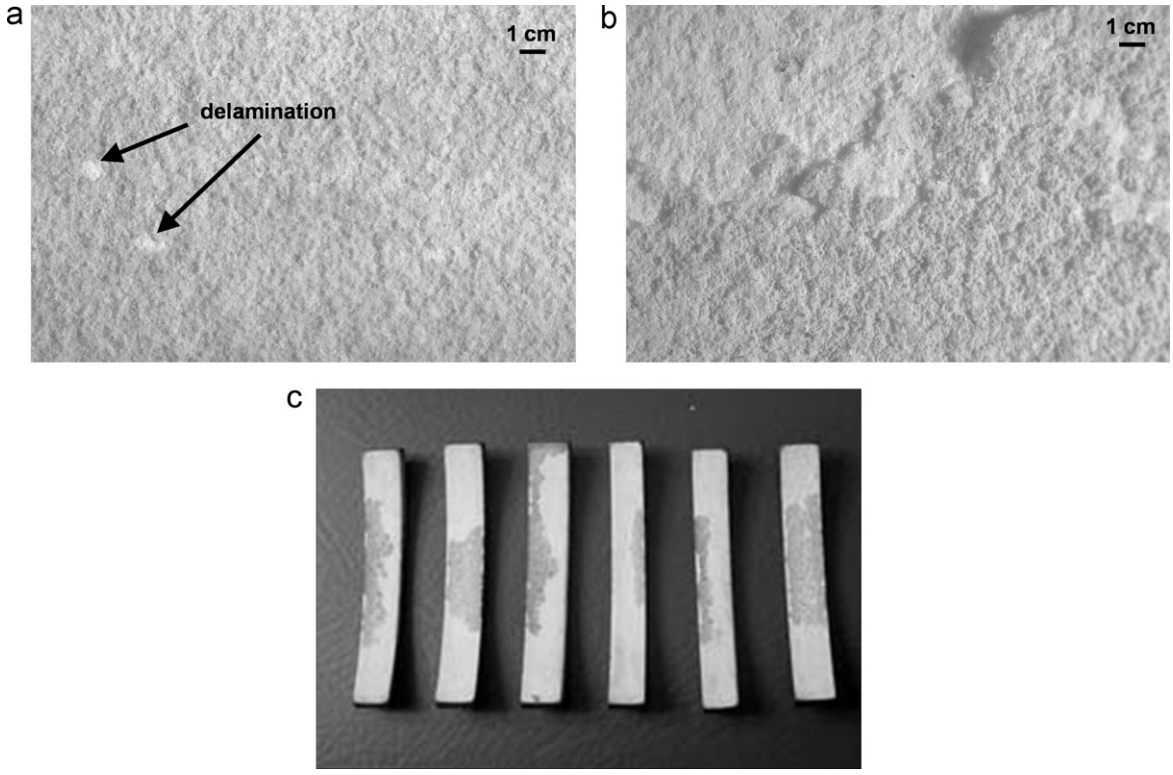

Fig. 8. (a) Shows the coating surface after 40–60 thermal shock cycles, while (b) shows the same surface after 90 cycles. Finally, (c) shows the state of thermally shocked specimens after 120 cycles.

cycles the nanostructured YSZ coatings result partially or completely delaminated, as shown in Fig. 8c.

The nanostructured zirconia coatings show higher thermal shock resistance than the conventional ones, as summarized in Table 3 [25,26]. The durability increases up to 60–80%. This enhancement can be explained in terms of higher porosity of nanostructured coatings as well as in terms of higher resistance to crack propagation. Indeed, the presence of porous nanosized areas increases the compliance and counteracts the sintering effects, thus partially preventing the densification of the porous microstructure.

These results are very promising when compared to those reported by other investigators for nanostructured and conventional zirconia coatings, as shown in Table 3. To this purpose, Liang and Ding [25] have reported an average porosity of 9% for their nanostructured 3YSZ coatings, whereas Wang et al. [26] have reported an average porosity of 10% for their nanostructured 8YSZ coatings showing a bimodal microstructure. In their works, the coatings have been heated at high temperature for 30 and 5 min, respectively, and then rapidly quenched in ambient temperature water. However, further key details should be known and carefully taken in account such as the substrate material, the bond coat and the characteristics of the starting feedstocks. The coating thickness and the slight differences in thermal shock test procedures can also affect the thermal shock resistance. As higher the thickness as higher the thermal stresses in the coating. From this point of view, nanostructured plasma sprayed YSZ coatings are very promising for TBC applications, due to their relatively low degree of degradation and high thermal shock cycling lifetime.

It has been reported that thermal exposure of nanostructured YSZ coatings at temperature higher than 1315 °C promotes enhanced grain growth and higher creep rate with respect to the conventional ones. This involves more rapid stress relaxation, promoting tensile stresses upon cooling and yielding to cracking and spallation [20]. Otherwise, Lima and Marple

Table 3
Thermal shock resistance of nanostructured and conventional YSZ coatings.

Coating	Thickness (μm)	Aging temperature (°C)	Number of cycles
Nanostructured YSZ	250	1020	80–90[a]
Conventional YSZ	250	1020	50[a]
Nanostructured YSZ [25]	200	1000	120
Conventional YSZ [25]	200	1000	48
Nanostructured YSZ [26]	300	1200	11
Conventional YSZ [26]	300	1200	2

[a] The number of cycles herein reported corresponds to the peeling of large areas from coating surface (the test has been stopped after 120 cycles).

[27] have more recently demonstrated that, by controlling the melting degree of the agglomerated particles, nanostructured coatings can be successfully engineered to counteract the sintering effects. Indeed, they exhibit a bimodal microstructure characterised by areas with different sintering rates. The retained porous nanozones exhibit higher driving force for sintering, so that they shrink at much faster rate, generating further voids within the microstructure and retarding the densification. The high toughness and the low Young's modulus of these coatings are able to increase the sintering resistance and the thermal cycling lifetime.

4. Conclusions

Nanostructured yttria-partially stabilized zirconia coatings were deposited by APS, in order to retain 20–25% of the starting nanostructure. They showed a complex microstructure composed of well-melted splats with columnar crystal structure, partially melted areas and equiaxed grains. The high retention of porous nanosized areas resulted in coatings with high porosity (>20%), which is suitable to reduce both the thermal conductivity and the stiffness. The microhardness of nanostructured YSZ coatings was slightly higher than that found for the conventional ones at 50 gf. When a load of 100 gf was applied the microhardness of nanostructured coatings significantly decreased, because the cohesive strength of retained nanosized areas was sensible to the indentation load. A bimodal distribution of mechanical properties was also noticed. Finally, an enhanced thermal shock resistance was found, because 90 cycles were needed to produce significant peeling of large areas from the coating surface, without spallation at top coat/bond coat interface. Future experiments will be devoted to the study of high-temperature sintering behaviour of nanostructured YSZ coatings.

References

[1] J.A. Nesbitt, Thermal response of various thermal barrier coatings in a high heat flux rocket engine, Surf. Coat. Technol. 43/44 (1990) 458–469.

[2] T.M. Yonushonis, Overview of thermal barrier coatings in diesel engines, J. Therm. Spray Technol. 6 (1) (1997) 50–56.

[3] X.Q. Cao, R. Vassen, D. Stöver, Ceramic materials for thermal barrier coatings, J. Eur. Ceram. Soc. 24 (2004) 1–10.

[4] C.R.C. Lima, E. Trevisan, Temperature measurements and adhesion properties of plasma sprayed thermal barrier coatings, J. Therm. Spray Technol. 8 (2) (1999) 323–327.

[5] M. Tamura, M. Takahashi, J. Ishii, K. Suzuki, M. Sato, K. Shimomura, Multilayered thermal barrier coatings for land-based gas turbines, J. Therm. Spray Technol. 8 (1) (1999) 68–72.

[6] P. Bengtsson, T. Ericsson, J. Wigren, Thermal shock testing of burner cans coated with a thick thermal barrier coating, J. Therm. Spray Technol. 7 (3) (1998) 340–348.

[7] J. Matejicek, S. Sampath, J. Dubsky, X-ray residual stress measurement in metallic and ceramic plasma sprayed coatings, J. Therm. Spray Technol. 7 (4) (1998) 489–496.

[8] J.S. Wallace, J. Ilavsky, Elastic modulus measurements in plasma sprayed deposits, J. Therm. Spray Technol. 7 (4) (1998) 521–526.

[9] M. Gell, Applying nanostructured materials to future gas turbine engines, J. Metals 46 (10) (1994) 30–34.

[10] R.S. Lima, B.R. Marple, Thermal spray coatings engineered from nanostructured ceramic agglomerated powders for structural, thermal barrier and biomedical applications: a review, J. Therm. Spray Technol. 16 (1) (2007) 40–63.

[11] J. Wu, H.B. Guo, L. Zhou, L. Wang, S.K. Gong, Microstructure and thermal properties of plasma sprayed thermal barrier coatings from nanostructured YSZ, J. Therm. Spray Technol. 19 (6) (2010) 1186–1194.

[12] H. Chen, X. Zhou, C. Ding, Investigation of the thermomechanical properties of a plasma-sprayed nanostructured zirconia coating, J. Eur. Ceram. Soc. 23 (9) (2003) 1449–1455.

[13] R. McPherson, A review of microstructure and properties of plasma sprayed ceramic coatings, Surf. Coat. Technol. 39/40 (1989) 173–181.

[14] L. Pawlowski, The Science and Engineering of Thermal Spray Coatings, John Wiley & Sons, New York, NY, 1995.

[15] R.S. Lima, A. Kucuk, C.C. Berndt, Integrity of nanostructured partially stabilized zirconia after plasma spray processing, Mater. Sci. Eng. A 313 (2001) 75–82.

[16] R.S. Lima, A. Kucuk, C.C. Berndt, Evaluation of microhardness and elastic modulus of thermally sprayed nanostructured zirconia coatings, Surf. Coat. Technol. 135 (2001) 166–172.

[17] H. Chen, Y. Zeng, C.X. Ding, Microstructural characterization of plasma-sprayed nanostructured zirconia powders and coatings, J. Eur. Ceram. Soc. 23 (2003) 491–497.

[18] P. Bengtsson, T. Johannesson, Characterization of microstructural defects in plasma-sprayed thermal barrier coatings, J. Therm. Spray Technol. 4 (1995) 245–251.

[19] R. McPherson, On the formation of thermally sprayed alumina coatings, J. Mater. Sci. 15 (1980) 3141–3149.

[20] R. Soltani, E. Garcia, T.W. Coyle, J. Mostaghimi, R.S. Lima, B.R. Marple, C. Moreau, Thermomechanical behaviour of nanostructured plasma sprayed zirconia coatings, J. Therm. Spray Technol. 15 (4) (2006) 657–662.

[21] G. Di Girolamo, C. Blasi, L. Pagnotta, M. Schioppa, Phase evolution and thermophysical properties of plasma sprayed thick zirconia coatings after annealing, Ceram. Int. 36 (2010) 2273–2280.

[22] H. Zhou, J. Wang, B. He, F. Li, J. Ma, B. De Sun, Mechanical properties of nanostructured zirconia coatings fabricated by air plasma spraying, Key Eng. Mater. 368/372 (2008) 1280–1283.

[23] C.K. Lin, C.C. Berndt, Statistical analysis of microhardness variations in thermal spray coatings, J. Mater. Sci. 30 (1995) 111–117.

[24] R.S. Lima, A. Kucuk, C.C. Berndt, Bimodal distribution of mechanical properties on plasma sprayed nanostructured partially stabilized zirconia, Mater. Sci. Eng. A 327 (2002) 224–232.

[25] B. Liang, C. Ding, Thermal shock resistance of nanostructured and conventional zirconia coatings deposited by atmospheric plasma spraying, Surf. Coat. Technol. 197 (2005) 185–192.

[26] W.Q. Wang, C.K. Sha, D.Q. Sun, X.J. Gu, Microstructural feature, thermal shock resistance and isothermal oxidation resistance of nanostructured zirconia coating, Mater. Sci. Eng. A 424 (2006) 1–5.

[27] R.S. Lima, B.R. Marple, Nanostructured YSZ thermal barrier coatings engineered to counteract sintering effects, Mater. Sci. Eng. A 485 (2008) 182–193.